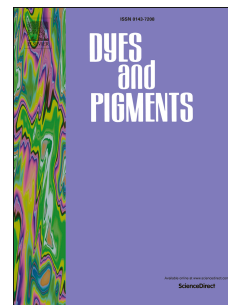


Journal Pre-proof

3-Benzoyl-4H-chromen-4-one: A Novel Twisted Acceptor for Highly Efficient Thermally Activated Delayed Fluorescence Emitters

Peng Wang, Junsheng Yu, Shanyong Chen, Hong Yu, Xingwu Yan, Youwei Guan, Jinlei Chen, Lu Li



PII: S0143-7208(20)31441-8

DOI: <https://doi.org/10.1016/j.dyepig.2020.108744>

Reference: DYPI 108744

To appear in: *Dyes and Pigments*

Received Date: 10 March 2020

Revised Date: 9 July 2020

Accepted Date: 26 July 2020

Please cite this article as: Wang P, Yu J, Chen S, Yu H, Yan X, Guan Y, Chen J, Li L, 3-Benzoyl-4H-chromen-4-one: A Novel Twisted Acceptor for Highly Efficient Thermally Activated Delayed Fluorescence Emitters, *Dyes and Pigments*, <https://doi.org/10.1016/j.dyepig.2020.108744>.

This is a PDF file of an article that has undergone enhancements after acceptance, such as the addition of a cover page and metadata, and formatting for readability, but it is not yet the definitive version of record. This version will undergo additional copyediting, typesetting and review before it is published in its final form, but we are providing this version to give early visibility of the article. Please note that, during the production process, errors may be discovered which could affect the content, and all legal disclaimers that apply to the journal pertain.

© 2020 Elsevier Ltd. All rights reserved.

Author Statement

In this work, the detailed contributions of each author are as following:

Peng Wang: Investigation, Methodology, Software

Junsheng Yu: Validation, Writing-Review & Editing

Shanyong Chen: Conceptualization, Formal analysis, Writing-Review & Editing

Hong Yu: Investigation

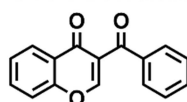
Xingwu Yan: Data Curation

Youwei Guan: Project administration, Writing-Original Draft

Jinlei Chen: Visualization, Supervision

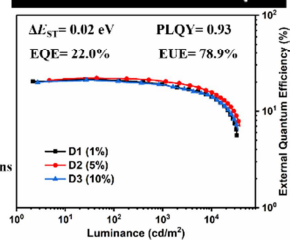
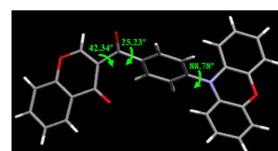
Lu Li: Resources, Writing-Review & Editing, Funding acquisition

Novel small and twisted acceptor



endow

- Nearly vertical D-A structure
- π - π interaction is prevented
- Abundant weak intermolecular interactions



3-Benzoyl-4H-chromen-4-one: A Novel Twisted Acceptor for Highly Efficient Thermally Activated Delayed Fluorescence Emitters

Peng Wang^{ab}, Junsheng Yu^a, Shanyong Chen^{*b}, Hong Yu^b, Xingwu Yan^b, Youwei Guan^b, Jinlei Chen^b, Lu Li^{*b}

^aState Key Laboratory of Electronic Thin Films and Integrated Devices, School of Optoelectronic Science and Engineering, University of Electronic Science and Technology of China (UESTC), Chengdu 610054, P. R. China

^bMicro/Nano Optoelectronic Materials and Devices International Science and Technology Cooperation Base of China, Chongqing University of Arts and Sciences, Chongqing 402160, P. R. China

*Corresponding Author. E-mail: chensy@cqwu.edu.cn (S. Chen) and lli@cqwu.edu.cn (L. Li).

Abstract

In this work, a novel twisted 3-benzoyl-4H-chromen-4-one (BZC) acceptor is reported and a BZC-based thermally activated delayed fluorescence (TADF) emitter, 3-(4-(10H-phenoxazin-10-yl)benzoyl)-4H-chromen-4-one (BZC-PXZ), is developed. The unique structure of BZC endows BZC-PXZ with favorable molecular and stacking structures. First, the small and twisted structure of BZC group not only brings about large dihedral angle (88.78°) between donor and acceptor groups, but also efficiently prevents $\pi\cdots\pi$ interaction. Second, the three oxygen atoms of BZC group bring about abundant weak intermolecular interactions which can enhance the charge-transporting ability of BZC-PXZ and facilitate the exciton recombination on it. As a result, BZC-PXZ exhibits small singlet-triplet energy splitting (0.02 eV) and high photoluminescence quantum yield (93%) simultaneously. Meanwhile, the BZC-PXZ-based device displays high efficiency (64.6 cd/A, 69.0 lm/W, 21.3%), high exciton utilization efficiency (77.2%) and low roll-off of efficiencies even at ultralow doped concentration of 1%. These results demonstrate that BZC group is a good acceptor for developing high-performance TADF emitters.

Keywords: Thermally activated delayed fluorescence; 3-Benzoyl-4H-chromen-4-one, Small singlet-triplet splitting; High photoluminescence quantum yield; Efficient exciton utilization

1. Introduction

As the third-generation emitter of organic light emitting diodes (OLEDs), thermally activated delayed fluorescence (TADF) emitter gains much attention in the past decade [1-11]. For TADF emitter, two parameters are most important: singlet-triplet splitting (ΔE_{ST}) and photoluminescence quantum yield (PLQY). Generally, small ΔE_{ST} and high PLQY are essential for efficient exciton utilization and high-performance TADF emitter. Previous studies indicate that the donor (D) and acceptor (A) composition groups play a vital role in determining ΔE_{ST} and PLQY[12-15]. For example, the combination of strong donor and strong acceptor can separate the highest occupied molecular orbital (HOMO) and lowest unoccupied molecular orbital (LUMO) to realize small ΔE_{ST} [16]. To meet the demand of TADF emitters, researchers have developed many donor and acceptor groups[17-22]. For donors, their choices are relatively fixed, including carbazole, aromatic amine, phenoxazine and their derivatives[23-24]. Hence, TADF studies mainly focus on developing new acceptors, molecular structures and exciplex-TADF[25-31]. In the past decade, many acceptors have been introduced, including cyanobenzene, pyrimidine, triazine, arylborane, etc[32-34]. Based on these acceptors, many excellent TADF emitters have been reported[35-39]. However, until now, TADF emitters have not been adopted in actual products because their performance need to be further improved. To realize this goal, new composition groups and molecular structures are needed. Therefore, developing novel acceptor for high-performance TADF emitters is still highly desired.

Herein, we report a novel 3-benzoyl-4H-chromen-4-one (BZC) acceptor and a BZC-based TADF emitter, 3-(4-(10H-phenoxazin-10-yl)benzoyl)-4H-chromen-4-one (BZC-PXZ) (**Scheme 1**). From the crystal structure of BZC-PXZ, it could be seen that BZC group was a small and twisted acceptor and the unique structure of BZC group could endow the material with favorable molecular and stacking structures. Photophysical measurements indicated that BZC-PXZ possessed small ΔE_{ST} (0.02 eV), high PLQY (93%) (measured in doped film, mCP: 5% BZC-PXZ) and short delayed fluorescence exciton lifetime (4.47 μ s). BZC-PXZ-based device displayed high performance. At the doped concentrations of 1%, 5% and 10%, the maximum external quantum efficiency (EQE) of devices were 21.3%, 22.0%, 20.9%, while the maximum exciton utilization efficiency (EUE) were 77.2%, 78.9%, 75.7%, respectively. These

results demonstrated that BZC group was a good acceptor for developing high-performance TADF emitters.

2. Experimental Section

2.1. General Information

All the starting chemicals for the synthesis were purchased from commercial sources and used as received without purification unless otherwise noted. All the solvents used for the synthesis were dried by sodium or calcium hydride and distilled under nitrogen atmosphere. ^1H NMR spectra were measured using an AVANCE 600 MHz spectrometer (Bruker). Mass spectrometry were measured by Shimadzu LCMS2020 instrument. Ultraviolet-visible (UV-Vis) absorption spectra were tested using a Hitachi U-3900 spectrophotometer. Fluorescence spectra were recorded using a Horiba FluoroMax-4 spectrophotometer spectrometer. The transient PL decay characteristic of the material was investigated using an Edinburgh Instruments FLS980 spectrometer. Thermal gravimetric analysis (TGA) and differential scanning calorimetry (DSC) characteristics were determined by a TA Q600 thermogravimeter and NETZSCH DSC204 instrument using the heating rate of $10\text{ }^\circ\text{C min}^{-1}$ under nitrogen atmosphere to obtain the compound weight loss. Cyclic voltammetry used an electrochemical workstation, the working electrode was a platinum electrode, the reference electrode was an Ag electrode, and the counter electrode was a platinum wire. The redox potential was measured in a 0.1 M solution at a scan rate of 100 mV s^{-1} with tetrabutylammonium hexafluorophosphate (TBAPF_6) as the electrolyte. The photoluminescence quantum yields (PLQYs) were measured with the Yokohama C9920-02G assay system. The transient photoluminescence decay characteristics of the doped film (mCP: 5% BZC-PXZ) was measured under nitrogen atmosphere at room temperature. According to the material properties, the excitation wavelength was 325 nm and the emission wavelength was 430 nm. Single-crystal diffraction data were collected on a Rigaku R-Axis-RAPID diffractometer using the ω -scan mode with graphite-monochromator $\text{Mo-K}\alpha$ radiation. The structure was solved with direct methods using the SHELXTL programs and refined with full-matrix least squares on F^2 . The crystal data can be obtained free of charge from the Cambridge Crystallographic Data Centre (CCDC: 1962908).

The vacuum sublimation was carried out at the sublimation machine from Shenyang Keyou

Vacuum Technology Co., Ltd. This machine had two heating sections to set up different temperatures. For BZC-PXZ, the two section temperatures were set to 120 and 220 °C, respectively. The vacuum pressure was 2.0×10^{-1} Pa. After 12 h, the sublimation finished and pure BZC-PXZ was obtained.

The DFT calculations were performed using Gaussian 09 program package. The geometrical structure was fully optimized with C1 symmetry constraints by using the restricted closed-shell B3LYP method with 6-31G* basis set. The lowest singlet (S_1) and lowest triplet (T_1) energies were evaluated based on a time-dependent DFT (TD-DFT) approach at B3LYP/6-31G* level.

2.2. OLED fabrication and characterization

All the devices were fabricated on indium tin oxide (ITO) substrate with a sheet resistance of 15 Ω/sq and a thickness of 135 nm. The ITO substrate was cleaned with acetone, detergent, distilled water in sequence, and then in an ultrasonic solvent bath. After dried at 80 °C for 1 h, the ITO substrates were treated with UV-ozone for 15 min. The substrate was transferred to a vacuum deposition chamber. HAT-CN, TAPC, TCTA, host-guest doped luminescent layer (mCP: BZC-PXZ), Bphen, LiF and aluminum were evaporated in sequence through a shadow mask with an array of 2.25 mm² under the pressure of 5.0×10^{-4} Pa. The current-voltage-luminance (J-V-L) characteristics were tested using a Keithley 2400 Semiconductor Characterization System and a calibrated silicon photodiode. The electroluminescent (EL) spectra and brightness were tested by a spectrograph PR-670. All the measurements were carried out under argon conditions at room temperature.

2.3. Synthesis

Methyl 4-(10H-phenoxazin-10-yl) benzoate (M1): To a two-necks round-bottom flask, 10H-phenoxazine (3.66 g, 20 mmol), methyl iodobenzoate (5.50 g, 21 mmol), cuprous oxide (6.00 g, 42 mmol) and dimethylacetamide (30 mL) were added. The mixture was stirred at 160 °C for 24 hours under nitrogen atmosphere. After cooling to room temperature, the mixture was filtrated and the filtrate was poured into 500 mL water and stirred for 10 min. The crude product was collected by filtration and purified by column chromatography on silica gel (eluent: petroleum/dichloromethane = 1:1) to provide a pale green solid (5.78 g, 90% yield). ¹H NMR (600 MHz, CDCl₃, δ): 8.26 (d, J = 8.2 Hz, 2H), 7.44 (d, J = 8.2 Hz, 2H), 6.70 (t, J = 5.8 Hz, 2H), 6.67 (t, J = 7.8 Hz, 2H), 6.59 (t, J = 7.3 Hz, 2H), 5.92 (d, J = 7.9 Hz, 2H), 3.97 (s, 3H).

HRMS: 317.1056 [M]⁺ (calcd: 317.11). Anal. Calcd for C₂₀H₁₅NO₃: C 75.70, H 4.76, N 4.41, O 15.12; found: C 75.58, H 4.77, N 4.43, O 15.20.

4-(10H-phenoxazin-10-yl) benzoic acid (M2): A mixture of M1 (4.82 g, 15 mmol), methanol (60 mL) and 1 M aqueous NaOH (60 mL) was stirred and refluxed for 6 hours under nitrogen atmosphere. After cooling to room temperature, the mixture was poured into 250 mL water and acidified by adding 1 M aqueous HCl until the pH of the mixture was adjusted to 5.0. The crude product was collected by filtration and purified by column chromatography on silica gel (eluent: petroleum/dichloromethane = 1:4) to provide a pale green solid (3.91 g, 86% yield). ¹H NMR (600 MHz, DMSO-*d*₆, δ): 13.18 (s, 1H), 8.20 (d, *J* = 7.5 Hz, 2H), 7.56 (d, *J* = 7.5 Hz, 2H), 6.77 (d, *J* = 7.3 Hz, 2H), 6.72-6.67 (m, 4H), 5.90 (d, *J* = 7.5 Hz, 2H). HRMS: 303.0884 [M]⁺ (calcd: 303.09). Anal. Calcd for C₁₉H₁₃NO₃: C 75.24, H 4.32, N 4.62, O 15.82; found: C 75.26, H 4.33, N 4.65, O 15.77.

2-Acetylphenyl 4-(9H-carbazol-9-yl) benzoate (M3): A mixture of M2 (3.64 g, 12 mmol), 3-acetyl-4-hydroxybenzene-1-ylum (1.5 mL, 13 mmol), 4-pyrrolidinopyridine (3.50 g, 5 mmol) and N, N-dicyclohexylcarbodiimide (7.00 g, 26 mmol) were added into 150 mL dry dichloromethane under nitrogen atmosphere. The mixture was stirred at room temperature for 12 hours. Then the mixture was filtrated and washed with 200 mL dichloromethane. The solvent was removed by rotary evaporation. The product was purified by column chromatography on silica gel (eluent: petroleum/dichloromethane = 1:2) to provide a yellow solid (4.20 g, 83% yield). ¹H NMR (600 MHz, CDCl₃, δ): 8.43 (d, *J* = 8.2 Hz, 1H), 7.90 (d, *J* = 6.3 Hz, 1H), 7.40-7.62 (m, 4H), 6.63-6.73 (m, 8H), 6.00 (d, *J* = 7.0 Hz, 2H), 2.60 (s, 3H). HRMS: 421.1278 [M]⁺ (calcd: 421.13). Anal. Calcd for C₂₇H₁₉NO₄: C 76.95, H 4.54, N 3.32, O 15.18; found: C 76.88, H 4.53, N 3.35, O 15.22.

1-(4-(10H-phenoxazin-10-yl) phenyl)-3-(2-hydroxyphenyl) propane-1, 3-dione (M4): The M3 (4.21 g, 10 mmol), KOH (672 mg, 12 mmol) were added into 150 mL dry pyridine and heated at 60 °C for 6 hours. After cooling to room temperature, water was added and the pH of the mixture was adjusted to 5.0 by adding 10% HCl. The product was collected by filtration and purified by column chromatography on silica gel (eluent: petroleum/dichloromethane = 1:2) to provide an orange solid (3.62 g, 86% yield). ¹H NMR (600 MHz, CDCl₃, δ): 15.53 (s, 1H), 12.06 (s, 1H), 8.17 (d, *J* = 8.5 Hz, 2H), 7.81 (d, *J* = 8.5 Hz, 1H), 7.50 (d, *J* = 6.8 Hz, 2H),

6.91-7.05 (m, 3H), 6.62-6.72 (m, 6H), 5.98 (d, $J = 7.9$ Hz, 2H), 4.70 (s, 1H). HRMS: 421.1277 $[M]^+$ (calcd: 421.13). Anal. Calcd for $C_{27}H_{19}NO_4$: C 76.95, H 4.54, N 3.32, O 15.18; found: C 76.93, H 4.54, N 3.33, O 15.19.

3-(4-(10H-phenoxazin-10-yl) benzoyl)-4H-chromen-4-one (BZC-PXZ): The mixture of M4 (2.11 g, 5 mmol), DMF-DMA (17 mL, 75 mmol) and toluene (100 mL) was heated at 80 °C for 1 hour. After cooling to room temperature, the product was collected by filtration and purified by column chromatography on silica gel (eluent: dichloromethane) to provide a yellow solid (1.98 g, 92% yield). 1H NMR (600 MHz, $CDCl_3$, δ): 8.39 (s, 1H), 8.29 (d, $J = 7.9$ Hz, 1H), 8.09 (d, $J = 7.9$ Hz, 2H), 7.78 (t, $J = 7.9$ Hz, 1H), 7.58 (d, $J = 8.5$ Hz, 1H), 7.52 (t, $J = 7.6$ Hz, 1H), 7.46 (d, $J = 7.9$ Hz, 2H), 6.60-6.72 (m, 6H), 6.02 (d, $J = 7.9$ Hz, 2H). ^{13}C NMR (600 MHz, $CDCl_3$, δ): 113.57, 115.64, 115.67, 118.42, 121.86, 123.33, 124.96, 125.07, 126.34, 126.47, 130.70, 130.72, 132.42, 134.60, 136.83, 144.05, 156.13, 159.08, 174.77, 190.96. HRMS: 432.1182 $[M+H]^+$ (calcd: 431.12). Anal. Calcd for $C_{28}H_{17}NO_4$: C 77.95, H 3.97, N 3.25, O 14.83; found: C 77.99, H 3.95, N 3.26, O 14.80.

3. Results and Discussion

3.1. Synthesis and Thermal Properties

BZC-PXZ was synthesized from phenoxazine and obtained as a yellow powder (**Scheme 1**). Then, it was further purified by column chromatography and vacuum sublimation. Finally, it was fully characterized by NMR, mass spectra and element analysis (**Fig. S1-S11**).

Thermal properties of BZC-PXZ were investigated using differential scanning calorimetry (DSC) and thermogravimetric analysis (TGA) (**Fig. S12 and Table 1**). From the DSC curve, no glass transition was observed. From the TGA curve, its decomposition temperature (T_d) (corresponding to 5% weight loss) was determined to be 303 °C. Good thermal stability is favorable for the formation of uniform thin films during thermal evaporation and prolongs the device operational lifetime.

3.2. Crystal Structure

The yellowish crystal of BZC-PXZ was obtained by slow vacuum sublimation and its single crystal structure was examined (**Fig. 1 and Table S2**). BZC-PXZ possesses a twisted molecular structure and the dihedral angles between different groups are shown in **Fig. 1b**. From left to

right (chromanone, carbonyl, benzene and phenoxazine), the dihedral angles are 42.34° , 25.23° and 88.78° , respectively. Obviously, the acceptor group, 3-benzoyl-4H-chromen-4-one, possesses twisted structure. BZC-PXZ molecules adopt a parallel arrangement model with four kinds of molecular rows. Within one molecular row, molecules connect with each other by C-H \cdots O and C-H \cdots π interactions with the contact distances of 2.685 Å and 3.123 Å respectively (yellow lines in **Fig. 1c**). Between different kinds of molecular rows, these rows connect with each other by C-H \cdots O, C-H \cdots π and $\pi\cdots\pi$ interactions (green lines in **Fig. 1c**). The contact distances of C-H \cdots O interactions are 2.552 Å, 2.559 Å and 2.705 Å respectively. The contact distance of $\pi\cdots\pi$ interaction is 3.727 Å with an overlap of half of a benzene ring. For C-H \cdots π interaction, its contact distances are 2.479 Å and 2.763 Å respectively. It can be seen that the small and twisted BZC group can not only endow BZC-PXZ with large dihedral angle (88.78°) between donor and acceptor groups, but also efficiently prevent the strong $\pi\cdots\pi$ interaction. Meanwhile, the oxygen atoms in BZC group bring about abundant weak intermolecular interactions.

The nearly vertical structure (dihedral angle: 88.78°) means efficient separation of donor and acceptor groups which is favorable for obtaining small ΔE_{ST} and efficient reverse intersystem crossing (RISC) process. The lack of $\pi\cdots\pi$ interaction can avoid fluorescence quenching and improve the fluorescent quantum efficiency. Finally, the intermolecular interactions can enhance the charge-transporting ability of BZC-PXZ and this is favorable for the exciton recombination on it.

3.3. Theoretical Calculations and Electrochemical Properties

To gain insight into the spatial distributions of the highest occupied molecular orbital (HOMO) and the lowest unoccupied molecular orbital (LUMO), density functional theory (DFT) calculations were carried out and results were shown in **Fig. 2a**. BZC-PXZ exhibited a prominent character of a typical TADF molecule: its HOMO was mainly located on phenoxazine group while its LUMO was mainly distributed on 3-benzoyl-4H-chromen-4-one group; there was only a little overlap between the HOMO and LUMO. The spatially separated frontier orbital distribution could reduce the ΔE_{ST} value and facilitate the reverse intersystem crossing from the lowest triplet excited state (T_1) to the lowest singlet excited state (S_1). The

HOMO and LUMO energy levels of BZC-PXZ were calculated to be -4.65 and -2.03 eV, respectively. The S_1 , T_1 and ΔE_{ST} were calculated to be 2.2431 eV, 2.1748 eV, 0.0683 eV, respectively. From the spectra below, the experimental S_1 , T_1 and ΔE_{ST} were 2.46 eV, 2.44 eV, 0.02 eV, respectively. Compared with experimental values, the calculated values exhibited similar variation tendency.

The electrochemical properties of BZC-PXZ were investigated by the cyclic voltammetry (CV) measurement in dichloromethane (**Fig. 2b**). BZC-PXZ showed reversible oxidation behavior. From the oxidation wave, its HOMO energy level was determined to be -5.05 eV according to the equation of $E_{HOMO} = - (E_{[onset, ox vs Fc^+/Fc]} + 4.8) \text{ eV}$. No reduction wave was observed. Its LUMO energy level was determined to be -2.42 eV from its HOMO and E_g .

3.4. Photophysical Properties

The UV-vis absorption spectra of BZC-PXZ in toluene was shown in **Fig. 3a**. The absorption below 350 nm could be ascribed to the local excitation transition absorption of 3-benzoyl-4H-chromen-4-one (BZC) and phenoxazine (PXZ). While the weak absorption around 408 nm was attributed to the charge-transfer transition from PXZ moiety to BZC moiety. From the absorption spectra, the energy gap between $S_{1,0}$ and $S_{0,0}$ (E_g) was estimated as 2.63 eV for BZC-PXZ. The absorption spectra of BZC-PXZ in different solvents were exhibited in **Fig. S15**. With the increase of solvent polarity, the charge-transfer transition absorption peaks were almost the same. This indicated that the ground-state dipole moment of BZC-PXZ was small.

To verify the lowest triplet excited state (T_1) of BZC-PXZ, its fluorescence and phosphorescence spectra in toluene at 77 K were measured (**Fig. 3a**). At room temperature, BZC-PXZ exhibited a broad emission with an unstructured peak of 561 nm. At 77 K, its emission showed a blue-shift with a single peak of 505 nm. From the crystal structure of BZC-PXZ, it could be seen that BZC-PXZ consisted of small composition groups and possessed twisted molecular structure. Hence, at room temperature, many molecular rotation and vibration happened. These unfavorable molecular motions consumed much energy. At 77 K, these motions stopped and those wasted energy could be used for light emission. Hence, compared with the emission peak at 300 K, the emission peak at 77 K showed an obvious blue-shift. For its phosphorescence spectra, no fine structure was observed, indicating that its T_1

state was not locally-excited (^3LE) state but was charge transfer (^3CT) state. From the peaks of fluorescence (505 nm) and phosphorescence (508 nm) spectra at 77 K, the S_1 and T_1 energy levels of BZC-PXZ were calculated to be 2.46 eV and 2.44 eV, respectively. Hence, its ΔE_{ST} was 0.02 eV. Small ΔE_{ST} facilitates the efficient RISC. The photoluminescence (PL) spectra of BZC-PXZ in crystalline state, pure-film state and doped-film state (mCP: 5% BZC-PXZ) were also measured (**Fig. S13**). Its fluorescence peaks at crystalline state, pure-film state and doped-film state were 596 nm, 589 nm, 533 nm, respectively. Compared with the solution and doped-film spectra, the pure-film and crystal spectra had a redshift which should be ascribed to the intermolecular interactions.

In order to investigate the TADF feature of BZC-PXZ, the transient photoluminescence (PL) decay characteristic of the doped film (mCP: 5% BZC-PXZ) was measured (**Fig. 3b**). The transient PL of BZC-PXZ showed clear secondary exponential decays with a nanosecond-scale prompt component and a microsecond-scale delayed component. The lifetimes of the prompt fluorescence (τ_p) and the delayed fluorescence (τ_d) were 21.59 ns and 4.47 μs , respectively. Meanwhile, to further confirm the TADF feature of BZC-PXZ, its temperature-dependent transient PL decays from 150 to 300 K were investigated (**Fig. S14**). With the increase of temperature, the delayed fluorescence intensity increased, indicating that the RISC process from the triplet to singlet excited states was enhanced by thermal activation. These results verified the TADF characteristic of BZC-PXZ. The PLQY of its doped film (mCP: 5% BZC-PXZ) was 93%. From the transient PL, the ratios of prompt component and delayed component were 52% and 48%, respectively, suggesting that the delayed fluorescence had a great contribution on the total fluorescence. In the film with mCP host, the PLQY of the prompt fluorescence (Φ_{PF}) and delayed fluorescence (Φ_{DF}) were 48% and 45%, respectively. The PLQYs of BZC-PXZ in dichloromethane (10^{-5} mol/L) and pure film were 0.86 and 0.21, respectively.

To investigate the charge transfer (CT) characteristic and the lowest singlet excited state (S_1) of BZC-PXZ, its photoluminescence (PL) spectra in different solvents (hexane, triethylamine, butylether, isopropylether, diethyl ether, ethyl acetate, dichloromethane, dimethylformamide, acetone, acetonitrile) were measured (**Fig. S15**). In hexane, the PL spectra of BCZ-PXZ exhibited a certain feature of vibrational structure, indicating that the fluorescence in hexane

contained the emission from locally excited state. In other solvents, the spectra exhibited a structure-less characteristic and vibration-free fine structure was observed. From hexane to acetonitrile, its emission peaks were 433 nm, 482 nm, 482 nm, 491 nm, 475 nm, 497 nm, 519 nm, 516 nm, 518 nm, 523 nm, respectively (**Table S1**). With the increase of solvent polarity, its emission peak showed a significant red-shift from 433 nm to 523 nm, indicating a remarkable CT character of excited state. According to Lippert-Mataga model [40], Stokes shift-solvent polarity curve was drawn to investigate the excited state (**Fig. S16**). With the increase of solvent polarity, the Stokes shift exhibited a straight line ($R = 0.97015$) and no inflection point was observed, further indicating that BZC-PXZ showed a CT-like character in both low-polarity and high-polarity solvents and the S_1 state of BZC-PXZ was 1CT .

To get insight into the dynamic processes of BZC-PXZ, the prompt-fluorescence (PF) rate constant (k_{PF}), the delayed-fluorescence (DF) rate constant (k_{DF}), the singlet radiative rate constant (k_r^S), the singlet nonradiative rate constant (k_{nr}^S), the intersystem crossing rate constant (k_{ISC}), the reverse intersystem crossing rate constant (k_{RISC}), the triplet nonradiative rate constant (k_{nr}^T), the intersystem crossing efficiency (Φ_{ISC}) and the reverse intersystem crossing efficiency (Φ_{RISC}) were calculated from the following equations [41]:

$$k_{PF} = \frac{\Phi_{PF}}{\tau_{PF}} \quad (1)$$

$$k_{DF} = \frac{\Phi_{DF}}{\tau_{DF}} \quad (2)$$

$$k_r^S = \Phi_{PF} \cdot k_{PF} \quad (3)$$

$$k_{nr}^S = k_{PF} - k_r^S - k_{PF} \frac{\Phi_{PF}}{\Phi_{PL}} \quad (4)$$

$$k_{ISC} = k_{PF} \frac{\Phi_{PF}}{\Phi_{PL}} \quad (5)$$

$$k_{RISC} = \frac{k_{DF} \cdot k_{PF} \cdot \Phi_{DF}}{k_{ISC} \cdot \Phi_{PF}} \quad (6)$$

$$k_{nr}^T = k_{DF} - \left(1 - \frac{k_{ISC}}{k_{PF}}\right) \cdot k_{RISC} \quad (7)$$

$$\Phi_{ISC} = \frac{k_{ISC}}{k_{PF}} \quad (8)$$

$$\Phi_{RISC} = \frac{k_{RISC}}{k_{RISC} + k_{nr}^T} \quad (9)$$

According to these equations, the k_{PF} , k_{DF} , k_r^S , k_{nr}^S , k_{ISC} , k_{RISC} , k_{nr}^T , Φ_{ISC} and Φ_{RISC} were $2.22 \times 10^7 \text{ s}^{-1}$, $1.01 \times 10^5 \text{ s}^{-1}$, $1.07 \times 10^7 \text{ s}^{-1}$, $8.61 \times 10^4 \text{ s}^{-1}$, $1.15 \times 10^7 \text{ s}^{-1}$, $1.83 \times 10^5 \text{ s}^{-1}$, $1.28 \times 10^4 \text{ s}^{-1}$,

0.52 and 0.94, respectively (**Table 2**). The magnitude of k_{RISC} was as high as 10^5 s^{-1} which verified the efficient RISC process.

3.5. Electroluminescent Properties

The crystal structure of BZC-PXZ indicated that BZC-PXZ might possess good charge-transporting ability. To investigate the charge-transporting ability of BZC-PXZ, the single-carrier devices with the structures of [ITO/BZC-PXZ (70 nm)/MoO₃ (10 nm)/Al] for hole-only and [ITO/TPBi (20 nm)/BZC-PXZ (60 nm)/LiF (1.5 nm)/Al] for electron-only were fabricated. Results were shown in **Fig. S17**. Based on the space charge limited current (SCLC) method and I–V characteristics, the hole and electron mobility of BZC-PXZ were determined to be $5.02 \times 10^{-5} \text{ cm}^2 \text{ V}^{-1} \text{ s}^{-1}$ and $2.06 \times 10^{-6} \text{ cm}^2 \text{ V}^{-1} \text{ s}^{-1}$, respectively. The good charge-transporting ability should be attributed to the abundant weak intermolecular interactions between BZC-PXZ molecules. Meanwhile, the electron mobility was close to the hole mobility, indicating that BZC-PXZ possessed good bipolar transporting ability. As is well known, balanced charge-transporting nature was favorable for the exciton recombination on it. Hence, for BZC-PXZ-based device, high performance can be expected.

To investigate the electroluminescent (EL) properties of BZC-PXZ, multilayer OLEDs with the structures of ITO/HAT-CN (15 nm)/TAPC (50 nm)/TCTA (5 nm)/mCP: xwt% BZC-PXZ (30 nm)/Bphen (45 nm)/LiF (1 nm)/Al (100 nm) (D1: 1wt%; D2: 5wt%; D3: 10wt%) were fabricated. The molecular structures in devices and their energy levels were shown in **Fig. 4**. In these devices, indium tin oxide (ITO), dipyrazino [2,3-f:2',3'-h] quinoxaline-2,3,6,7,10,11-hexacarbonitrile (HAT-CN), 4,4'-cyclohexylidenebis [N, N-bis (p-tolyl) aniline] (TAPC), 4,4',4''-tris (carbazol-9-yl)-triphenylamine (TCTA), 1,3-bis-9H-carbazol-9-ylbenzene (mCP), 4,7-diphenyl-1,10-phenanthroline (Bphen), lithium fluoride (LiF) and aluminium (Al) were utilized as the anode, hole-injection layer, hole-transporting layer, electron-blocking layer, host, electron-transporting layer, electron-injection layer and cathode, respectively. BZC-PXZ was doped in mCP as the emitting layer. The current density-voltage-luminance (J-V-L) characteristics, efficiencies *versus* luminance curves, EL spectra as well as external quantum efficiencies (EQE) were shown in **Fig. 5** and **Table 3**.

As shown in **Fig. 5** and **Table 3**, these devices exhibited green emission and no emission

peak of host was observed even at low doped concentration of 1%, indicating the complete energy transfer from host to BZC-PXZ (**Fig. 5a**). With the increase of doped concentration, the emission peak had a small redshift from 542 nm to 546 nm which should be attributed to the enhanced intermolecular interaction. With the variation of driving voltage, the EL spectra exhibited good stabilities that were important for high performance displays and lighting sources. Because of the direct charge trap of BZC-PXZ, these devices had low turn-on voltage (about 2.7 V) regardless of the doped concentration. Meanwhile, the increased luminance features of devices were not affected by the doped concentration yet and their maximum brightness exceeded 33000 cd/m² (**Fig. 5b**).

The maximum brightness (L_{\max}), maximum external quantum efficiency ($\eta_{\text{ext.max}}$), current ($\eta_{\text{c.max}}$) and power ($\eta_{\text{p.max}}$) efficiencies of these three devices were shown in **Table 3**. With the increase of doped concentration from 1% to 10%, the devices displayed similar performance: 64.6 cd/A, 69.0 lm/W and 21.3% for D1; 66.5 cd/A, 70.6 lm/W and 22.0% for D2; 63.5 cd/A, 66.8 lm/W and 20.9% for D3. The high device efficiencies should be ascribed to the unique structure of BZC acceptor. Because of the small and twisted BZC group, the donor was almost perpendicular to the acceptor and $\pi\cdots\pi$ interaction was efficiently prevented. Hence, BZC-PXZ exhibited small ΔE_{ST} (0.02 eV) and high PLQY (0.92-0.93, the emitting layers) simultaneously which made it possess high utilization efficiencies of singlet and triplet excitons (**Table 3**). These devices exhibited low roll-off of efficiencies (**Fig. 5 and Table 3**). Except for the above reason, the intermolecular interactions might be another reason for the low roll-off of efficiencies. BZC group possessed three oxygen atoms which brought about abundant weak intermolecular interactions (**Fig. 1**) that could enhance the charge-transporting ability of BZC-PXZ. From the single-carrier devices, its hole and electron mobility were determined to be $5.02 \times 10^{-5} \text{ cm}^2 \text{ V}^{-1} \text{ s}^{-1}$ and $2.06 \times 10^{-6} \text{ cm}^2 \text{ V}^{-1} \text{ s}^{-1}$, respectively. The high and balanced charge-transporting ability was favorable for the exciton recombination on it to obtain high efficiency and low roll-off of efficiency.

To evaluate the exciton utilization efficiency (η_{EUE}) of BZC-PXZ, the η_{EUE} of these three devices were calculated according to the following equation [42]:

$$\text{EQE} = \eta_{\text{IQE}} \times \eta_{\text{out}} = \eta_{\text{he}} \times \Phi_{\text{PL}} \times \eta_{\text{EUE}} \times \eta_{\text{out}}$$

Here, η_{IQE} was the internal quantum efficiency, η_{out} was the light out-coupling efficiency

(0.2-0.3), η_{hc} was the electron-hole recombination efficiency which was usually set as 100%, Φ_{PL} was the photoluminescence quantum yield of emitting layer. If η_{out} was assumed to be 0.3, the maximum η_{EUE} of D1, D2 and D3 were 77.2%, 78.9% and 75.7%, respectively. The η_{EUE} was about 3 times higher than the theoretical limit of 25% for conventional fluorescent emitters, indicating that most of triplet exciton was transformed into singlet exciton for light harvesting.

4. Conclusions

In summary, we reported a novel 3-benzoyl-4H-chromen-4-one (BZC) acceptor whose unique structure could endow the material with favorable molecular and stacking structures. For molecular structure, the twisted BZC group brought about nearly vertical structure between donor and acceptor groups. For stacking structure, because of the three oxygen atoms and structure of BZC group, abundant weak intermolecular interactions could be formed but $\pi\cdots\pi$ interaction was prevented. Based on BZC group, a TADF emitter, BZC-PXZ, was developed. BZC-PXZ exhibited small ΔE_{ST} (0.02 eV) and high PLQY (93%) simultaneously. Meanwhile, the BZC-PXZ-based device displayed high efficiency (64.6 cd/A, 69.0 lm/W, 21.3%), high exciton utilization efficiency (77.2%) and low roll-off of efficiencies even at ultralow doped concentration of 1%. These results demonstrated that BZC group was a good acceptor for developing high-performance TADF emitters.

Acknowledgments

This work was supported by National Key Research and Development Project of China (2018YFB0407100-02), National Natural Science Foundation of China (51903026, 61505018, U1663229, 21603020, 61705026, 51903027), the China Postdoctoral Science Foundation (2019 M653375), Financial Projects of Sichuan Science and Technology Department (2018ZYZF0062), Natural Science Foundation of Chongqing Science & Technology Commission (cstc2017zdcy-yszxX0004, cstc2019jcyjqq0092, cstc2016jcyjjs0006, cstc2016jcyjA0148, cstc2018jszx-cydzX0137, cstc2016jcyjA0577, cstc2018jcyjAX0212, cstc2017jcyjAX0097), Science and Technology Innovation Leader Plan of Chongqing (T04040012), Science and Technology Research Program of Chongqing Municipal Education Commission (KJQN201901314, KJZD-K201901302, KJ1711269), Natural Science Foundation

of Yongchuan District (Ycstc, 2018nb0601, 2019nc0601), the Chongqing University Outstanding Achievement Transformation Projects (KJZH17130), Overseas Returnees Support Program for Innovation and Entrepreneurship of Chongqing (cx2018136). This work is also sponsored by Sichuan Province Key Laboratory of Display Science and Technology.

References

- [1] Huang WL, Einzinger M, Zhu TY, Chae HS, Jeon S, Ihn SG, et al. Molecular design of deep blue thermally activated delayed fluorescence materials employing a homoconjugative triptycene scaffold and dihedral angle tuning. *Chem Mater*. 2018;30(5):1462-6.
- [2] Li HF, Hong MK, Scarpaci A, He XY, Risko C, Sears JS, et al. Chemical stabilities of the lowest triplet state in aryl sulfones and aryl phosphine oxides relevant to OLED applications. *Chem Mater*. 2019;31(5):1507-19.
- [3] Liang J, Li CL, Zhuang XM, Ye KQ, Liu Y, Wang Y. Novel blue bipolar thermally activated delayed fluorescence material as host emitter for high-efficiency hybrid warm-white OLEDs with stable high color-rendering index. *Adv Funct Mater*. 2018;28(17):1707002.
- [4] Venkatramaiah N, Kumar GD, Chandrasekaran Y, Ganduri R, Patil S. Efficient blue and yellow organic light-emitting diodes enabled by aggregation-induced emission. *ACS Appl Mater Interfaces*. 2018;10(4):3838-47.
- [5] Delgado-Aguilar M, Oliver-Ortega H, Alberto Mendez J, Camps J, Espinach FX, Mutje P. The role of lignin on the mechanical performance of polylactic acid and jute composites. *Int J Biol Macromol*. 2018;116:299-304.
- [6] Chen JX, Tao WW, Xiao YF, Tian S, Chen WC, Wang K, et al. Isomeric thermally activated delayed fluorescence emitters based on indolo[2,3-*b*]acridine electron-donor: a compromising optimization for efficient orange-red organic light-emitting diodes. *J Mater Chem C*. 2019;7(10):2898-904.
- [7] Wu K, Zhang T, Wang Z, Wang L, Zhan L, Gong S, et al. De novo design of excited-state intramolecular proton transfer emitters via a thermally activated delayed fluorescence channel. *J Am Chem Soc*. 2018;140(28):8877-86.
- [8] Yu L, Wu ZB, Xie GH, Zhong C, Zhu ZC, Ma DG, et al. An efficient exciton harvest route for high-performance OLEDs based on aggregation-induced delayed fluorescence. *Chem*

Commun. 2018;54(11):1379-82.

[9] Xie GH, Luo JJ, Huang ML, Chen TH, Wu KL, Gong SL, et al. Inheriting the characteristics of TADF small molecule by side-chain engineering strategy to enable bluish-green polymers with high PLQYs up to 74% and external quantum efficiency over 16% in light-emitting diodes. *Adv Mater.* 2017;29(11):1604223.

[10] Yu L, Wu ZB, Zhong C, Xie GH, Wu KL, Ma DG, et al. Tuning the emission from local excited-state to charge-transfer state transition in quinoxaline-based butterfly-shaped molecules: Efficient orange OLEDs based on thermally activated delayed fluorescence emitter. *Dyes Pigments.* 2017;141:325-32.

[11] Zeng WX, Lai HY, Lee WK, Jiao M, Shiu YJ, Zhong C, et al. Achieving nearly 30% external quantum efficiency for orange-red organic light emitting diodes by employing thermally activated delayed fluorescence emitters composed of 1,8-naphthalimide-acridine hybrids. *Adv Mater.* 2018;30(5):1704961.

[12] Xie ZL, Su TT, Ubba E, Deng HJ, Mao Z, Yu T, et al. Achieving tunable dual-emissive and high-contrast mechanochromic materials by manipulating steric hindrance effects. *J Mater Chem C.* 2019;7(11):3300-5.

[13] Zhao HB, Wang ZH, Cai XY, Liu KK, He ZZ, Liu X, et al. Highly efficient thermally activated delayed fluorescence materials with reduced efficiency roll-off and low on-set voltages. *Mater Chem Front.* 2017;1(10):2039-46.

[14] Chen SY, Wei JB, Wang K, Wang CG, Chen D, Liu Y, et al. Constructing high-performance blue, yellow and red electroluminescent devices based on a class of multifunctional organic materials. *J Mater Chem C.* 2013;1(40):6594-602.

[15] Chapran M, Pander P, Vasyliieva M, Wiosna-Salyga G, Ulanski J, Dias FB, et al. Realizing 20% external quantum efficiency in electroluminescence with efficient thermally activated delayed fluorescence from an exciplex. *ACS Appl Mater Interfaces.* 2019;11(14):13460-71.

[16] Im Y, Kim M, Cho YJ, Seo J-A, Yook KS, Lee JY. Molecular design strategy of organic thermally activated delayed fluorescence emitters. *Chem Mater.* 2017;29(5):1946-63.

[17] Yang Z, Mao Z, Xu C, Chen XJ, Zhao J, Yang ZY, et al. A sterically hindered asymmetric D-A-D' thermally activated delayed fluorescence emitter for highly efficient non-doped organic light-emitting diodes. *Chem Sci.* 2019;10(35):8129-34.

- [18] Liu ZW, Song FL, Shi WB, Gurzadyan G, Yin HY, Song B, et al. Nitroreductase-activatable theranostic molecules with high PDT efficiency under mild hypoxia based on a TADF fluorescein derivative. *ACS Appl Mater Interfaces*. 2019;11(17):15426-35.
- [19] Braveenth R, Bae IJ, Raagulan K, Kim S, Kim S, Kim M, et al. Dibenzothiophene-indolocarbazole-based bipolar material: host for green phosphorescent OLEDs and non-doped fluorescent emitter. *Dyes Pigments*. 2019;162:466-74.
- [20] Rajamalli P, Chen DY, Li WB, Samuel IDW, Cordes DB, Slawin AMZ, et al. Enhanced thermally activated delayed fluorescence through bridge modification in sulfone-based emitters employed in deep blue organic light-emitting diodes. *J Mater Chem C*. 2019;7(22):6664-71.
- [21] Zhang WJ, Zhou ZX, Liu L, Zhong XX, Asiri AM, Alamry KA, et al. Highly-efficient blue neutral mononuclear copper(I) halide complexes containing bi- and mono-dentate phosphine ligands. *J Lumin*. 2018;196:425-30.
- [22] Li W, Zhao JW, Li LJ, Du XY, Fan C, Zheng CJ, et al. Efficient solution-processed blue and white OLEDs based on a high-triplet bipolar host and a blue TADF emitter. *Org Electron*. 2018;58:276-82.
- [23] Chen Z, Li H, Tao Y, Chen L, Chen C, Jiang H, et al. Tuning intramolecular conformation and packing mode of host materials through noncovalent interactions for high-efficiency blue electrophosphorescence. *ACS Omega*. 2019;4(5):9129-34.
- [24] Oh CS, Lee HL, Hong WP, Lee JY. Benzothienopyrimidine as a co-planar type rigid acceptor for high external quantum efficiency in thermally activated delayed fluorescence Emitters. *J Mater Chem C*. 2019;7(25):7643-53.
- [25] Yu L, Wu ZB, Xie GH, Zeng WX, Ma DG, Yang CL. Molecular design to regulate the photophysical properties of multifunctional TADF emitters towards high-performance TADF-based OLEDs with EQEs up to 22.4% and small efficiency roll-offs. *Chem Sci*. 2018;9(5):1385-91.
- [26] Konidena RK, Lee KH, Lee JY, Hong WP. 15H-diindolo[2,3-b:1',2',3'-lm]carbazole: a novel rigid donor for highly efficient thermally activated delayed fluorescence emitters. *J Mater Chem C*. 2019;7(26):8037-44.
- [27] Sarma M, Wong KT. Exciplex: an intermolecular charge-transfer approach for TADF. *ACS Appl Mater Interfaces*. 2018;10(23):19279-304.

- [28] Liu XK, Chen Z, Zheng CJ, Liu CL, Lee CS, Li F, et al. Prediction and design of efficient exciplex emitters for high-efficiency, thermally activated delayed-fluorescence organic light-emitting diodes. *Adv Mater.* 2015;27(14):2378-83.
- [29] Goushi K, Yoshida K, Sato K, Adachi C. Organic light-emitting diodes employing efficient reverse intersystem crossing for triplet-to-singlet state conversion. *Nat Photonics.* 2012;6(4):253-8.
- [30] Cao HT, Zhao Y, Sun C, Fang D, Xie LH, Yan MN, et al. Novel electron acceptor based on Spiro fluorine-9,9'-xanthene for exciplex thermally activated delayed fluorescence. *Dyes Pigments.* 2018;149:422-9.
- [31] Zhang M, Liu W, Zheng CJ, Wang K, Shi YZ, Li X, et al. Tricomponent exciplex emitter realizing over 20% external quantum efficiency in organic light-emitting diode with multiple reverse intersystem crossing channels. *Adv Sci.* 2019;6(14):1801938.
- [32] Wang BY, Qiao XF, Yang Z, Wang YF, Liu SZ, Ma DG, et al. Realizing efficient red thermally activated delayed fluorescence organic light-emitting diodes using phenoxazine/phenothiazine-phenanthrene hybrids. *Org Electron.* 2018;59:32-8.
- [33] Zhao J, Chen XJ, Yang Z, Chi ZH, Yang ZY, Zhang Y, et al. Highly-efficient fully non-doped white organic light-emitting diodes consisting entirely of thermally activated delayed fluorescence emitters. *J Mater Chem C.* 2018;6(13):3226-32.
- [34] Wu ZG, Yan ZP, Luo XF, Yuan L, Liang WQ, Wang Y, et al. Non-doped and doped circularly polarized organic light-emitting diodes with high performances based on chiral octahydro-binaphthyl delayed fluorescent luminophores. *J Mater Chem C.* 2019;7(23):7045-52.
- [35] Liu D, Tian WW, Feng YL, Zhang XS, Ban XX, Jiang W, et al. Achieving 20% external quantum efficiency for fully solution-processed organic light-emitting diodes based on thermally activated delayed fluorescence dendrimers with flexible chains. *ACS Appl Mater Interfaces.* 2019;11(18):16737-48.
- [36] Fan XC, Wang K, Zheng CJ, Dai GL, Shi YZ, Li YQ, et al. Thermally activated delayed fluorescence emitters with low concentration sensitivity for highly efficient organic light emitting devices. *J Mater Chem C.* 2019;7(29):8923-8.
- [37] Wu TL, Liao SY, Huang PY, Hong ZS, Huang MP, Lin CC, et al. Exciplex organic light-emitting diodes with nearly 20% external quantum efficiency: effect of intermolecular

steric hindrance between the donor and acceptor pair. *ACS Appl Mater Interfaces*. 2019;11(21):19294-300.

[38] Li NQ, Fang YY, Li L, Zhao HR, Quan YW, Ye SH, et al. A universal solution-processable bipolar host based on triphenylamine and pyridine for efficient phosphorescent and thermally activated delayed fluorescence OLEDs. *J Lumin*. 2018;199:465-74.

[39] Park SY, Choi S, Park GE, Kim HJ, Lee C, Moon JS, et al. Unconventional three-armed luminogens exhibiting both aggregation-induced emission and thermally activated delayed fluorescence resulting in high-performing solution-processed organic light-emitting diodes. *ACS Appl Mater Interfaces*. 2018;10(17):14966-77.

[40] Zhang ST, Yao L, Peng QM, Li WJ, Pan YY, Xiao R, et al. Achieving a significantly increased efficiency in nondoped pure blue fluorescent OLED: a quasi-equivalent hybridized excited state. *Adv Funct Mater*. 2015;25(11):1755-62.

[41] Li CY, Duan CB, Han CM, Xu H. Secondary acceptor optimization for full-exciton radiation: toward sky-blue thermally activated delayed fluorescence diodes with external quantum efficiency of approximate to 30%. *Adv Mater*. 2018;30(50):1804228.

[42] Wei XF, Li ZY, Hu TP, Duan RH, Liu JJ, Wang RF, et al. Substitution conformation balances the oscillator strength and singlet-triplet energy gap for highly efficient D-A-D thermally activated delayed fluorescence emitters. *Adv Optical Mater*. 2019;7(11):1801767.

Figure and table captions

Scheme 1. The synthetic procedures of BZC-PXZ.

Fig. 1. a) The molecular structure with 50% thermal ellipsoids. b) The dihedral angles between different groups in BZC-PXZ. c) The packing structure of BZC-PXZ.

Fig. 2. a) Frontier-molecular-orbital distributions, energy levels, and HOMO-LUMO energy gap for BZC-PXZ characterized by DFT calculations. b) Cyclic voltammetry (CV) curve of BZC-PXZ in dichloromethane.

Fig. 3. a) Absorption spectra, fluorescence spectra (at 300 K and 77K) and phosphorescence spectra (at 77 K) of BZC-PXZ in toluene (1.0×10^{-4} mol/L). b) Transient PL decay profile of BZC-PXZ-doped mCP film (5wt%); Inset: decay measured over a time range of 200 ns.

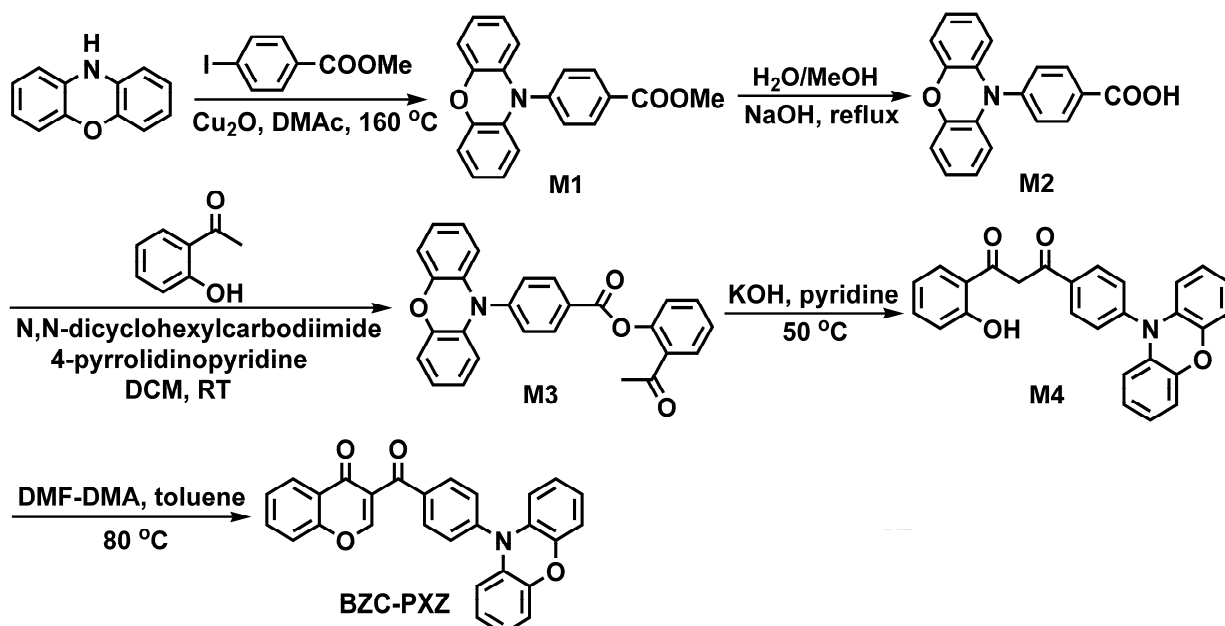
Fig. 4. a) Energy level diagram and b) chemical structures of the materials used in OLEDs.

Fig. 5. a) EL spectra of D1, D2 and D3 at the luminance of 1000 cd/m². b) Current density-voltage-luminance (J-V-L) curves of D1, D2 and D3. c) Current efficiency-luminance-power efficiency (CE-L-PE) curves of D1, D2 and D3. d) External quantum efficiency-luminance curves of D1, D2 and D3.

Table 1. Photophysical and electrochemical properties of BZC-PXZ.

Table 2. Photophysical properties of BZC-PXZ-doped mCP film (doped concentration: 5%).

Table 3. The electroluminescent performance of BZC-PXZ-doped devices.



Scheme 1.

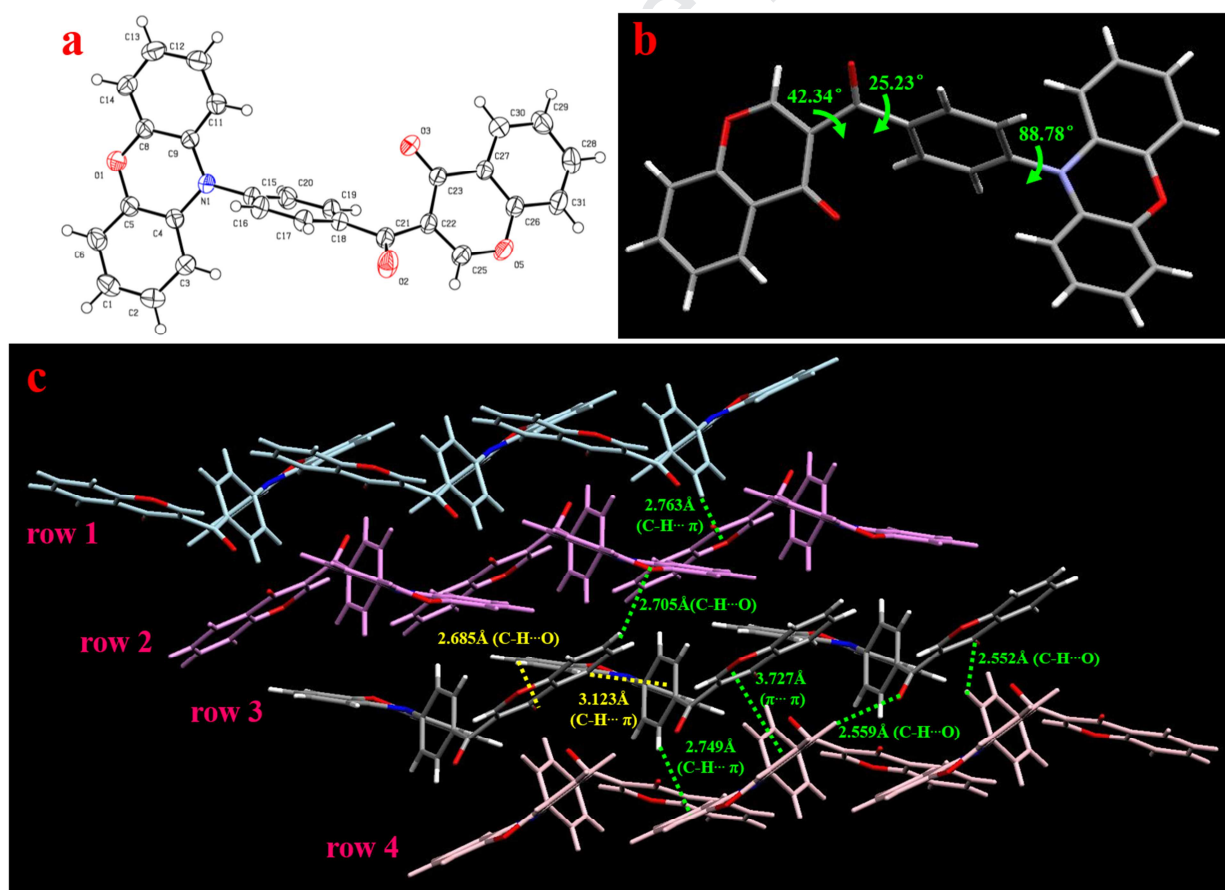


Fig. 1.

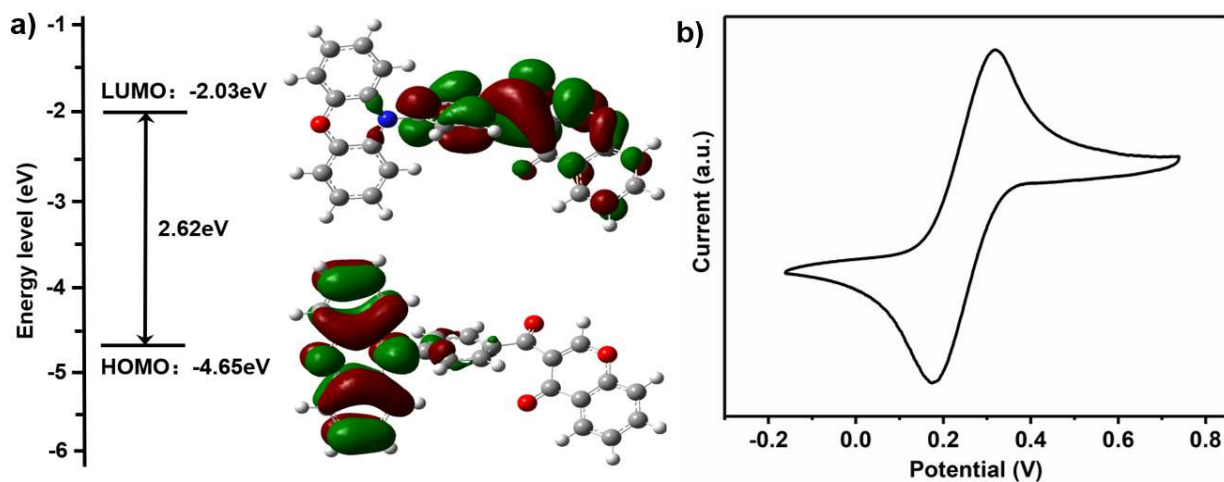


Fig. 2.

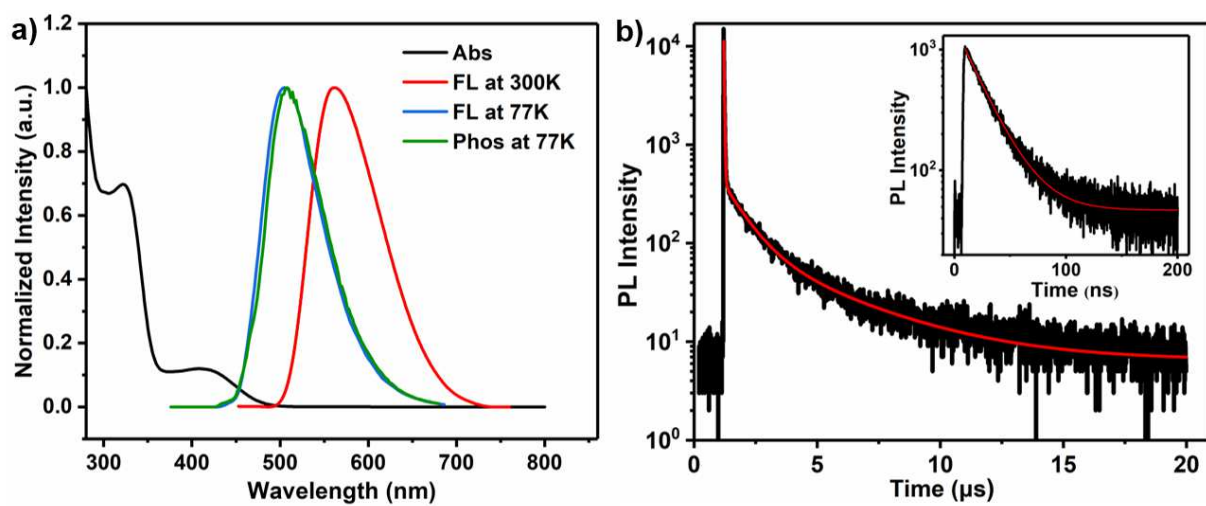


Fig. 3.

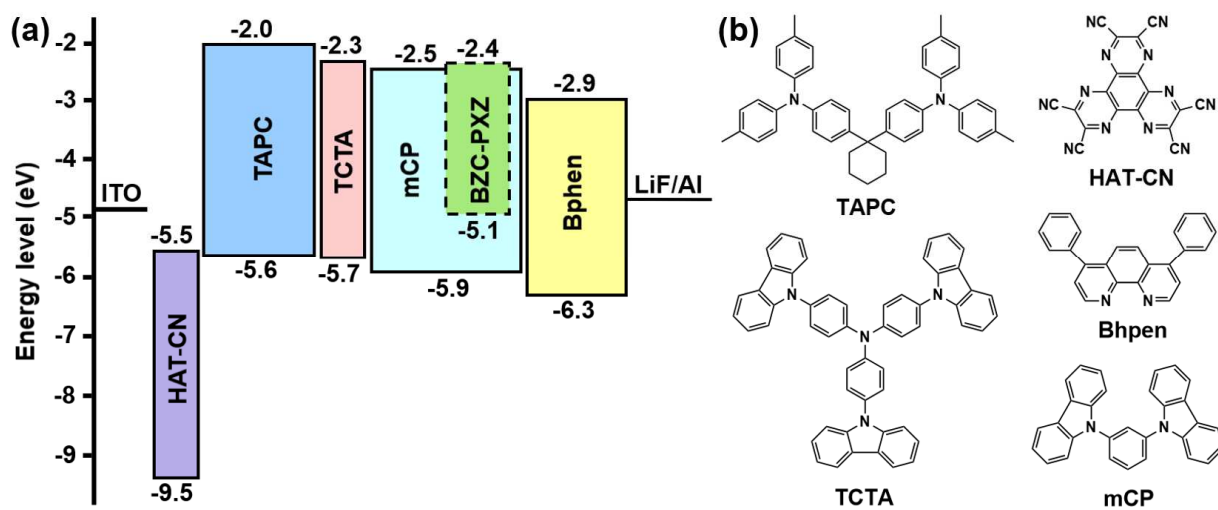


Fig. 4.

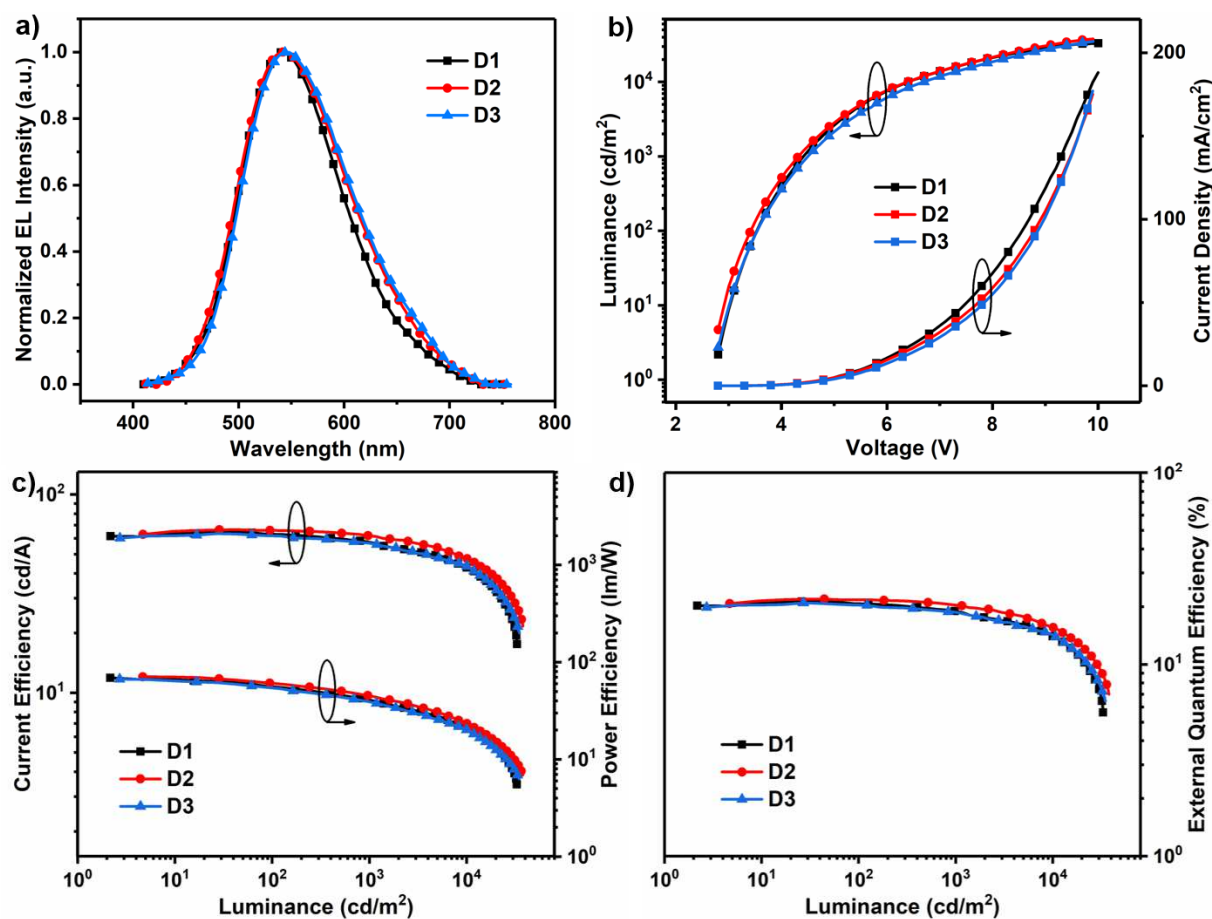


Fig. 5.

Table 1. Photophysical and electrochemical properties of BZC-PXZ.

Compound	$T_d^a)$ [°C]	$\lambda_{abs}^b)$ [nm]	$\lambda_{PL}^b)$ [nm]	Φ_{PL} film ^{c)}	$\tau_p^d)$ [ns]	$\tau_d^d)$ [μs]	HOMO/LUMO [eV]	$E_S/E_T^e)$ [eV]	ΔE_{ST} [eV]
BZC-PXZ	303	325/408	561	0.93	21.59	4.47	-5.05/-2.42	2.46/2.44	0.02

^{a)} T_d : decomposition temperature corresponding to 5% weight loss. ^{b)} Measured in toluene at room temperature. ^{c)} Measured in doped film (mCP: 5% BZC-PXZ). ^{d)} PL lifetimes of prompt (τ_p) and delayed (τ_d) decay components for doped film (mCP: 5% BZC-PXZ) at room temperature. ^{e)} Singlet (E_S) and triplet (E_T) energies measured in the diluted toluene solution and estimated from the peaks of the fluorescence and phosphorescence spectra (at 77 K), respectively.

Table 2. Photophysical properties of BZC-PXZ-doped mCP film (doped concentration: 5%).

Dopant	$\Phi_{PF}^{a)}$	$\Phi_{DF}^{b)}$	$\Phi_{ISC}^{c)}$	$\Phi_{RISC}^{d)}$	$k_{PF}^{e)}$	$k_{DF}^{f)}$	$k_r^{g)}$	$k_{nr}^s{}^{h)}$	$k_{nr}^T{}^{i)}$	$k_{ISC}^{j)}$	$k_{RISC}^{k)}$
					[10 ⁷ s ⁻¹]	[10 ⁵ s ⁻¹]	[10 ⁷ s ⁻¹]	[10 ⁴ s ⁻¹]	[10 ⁴ s ⁻¹]	[10 ⁷ s ⁻¹]	[10 ⁵ s ⁻¹]
BZC-PXZ	0.48	0.45	0.52	0.94	2.22	1.01	1.07	8.61	1.28	1.15	1.83

^{a)} Prompt fluorescence efficiency. ^{b)} Delayed fluorescence efficiency. ^{c)} Intersystem crossing efficiency. ^{d)} Reverse intersystem crossing efficiency. ^{e)} Prompt-fluorescence rate constant. ^{f)} Delayed-fluorescence rate constant. ^{g)} Singlet radiative rate constant. ^{h)} Singlet nonradiative rate constant. ⁱ⁾ Triplet nonradiative rate constant. ^{j)} Intersystem crossing rate constant. ^{k)} Reverse intersystem crossing rate constant.

Table 3. The electroluminescent performance of BZC-PXZ-doped devices.

Device	$V_{on}^{a)}$	$L_{max}^{b)}$	CE[cd/A]/PE[lm/W]/EQE[%] ^{c)}			$\eta_{EUE, max}^{e)}$	$\Phi^{f)}$
			Maximum	1000 cd m ⁻²	Roll-off rate (%) ^{d)}		
D1 (1wt%)	2.6	33114	64.6/69.0/21.3	57.6/41.1/18.9	10.8/40.4/11.3	77.2%	0.92
D2 (5wt%)	2.7	37729	66.5/70.6/22.0	61.5/43.9/20.4	7.5/37.8/7.3	78.9%	0.93
D3 (10wt%)	2.7	35024	63.5/66.8/20.9	56.8/39.2/18.7	10.6/41.3/10.5	75.7%	0.92

^{a)} V_{on} : voltage recorded at 1 cd m⁻². ^{b)} Maximum luminescence. ^{c)} CE: current efficiency; PE: power efficiency; EQE: external quantum efficiency. ^{d)} The efficiency variation rate from maximum efficiency to efficiency at 1000 cd m⁻². ^{e)} $\eta_{EUE, max}$: maximum exciton utilization efficiency. ^{f)} PLQY of BZC-PXZ-doped mCP film with different concentrations.

1. A novel twisted 3-benzoyl-4H-chromen-4-one (BZC) acceptor is reported.
2. The unique structure of BZC group can endow the material with favorable molecular and stacking structures.
3. BZC-based thermally activated delayed fluorescence emitter, BZC-PXZ, displays high performance in devices.

Journal Pre-proof

Declaration of interests

The authors declare that they have no known competing financial interests or personal relationships that could have appeared to influence the work reported in this paper.

The authors declare the following financial interests/personal relationships which may be considered as potential competing interests:

Journal Pre-proof